

## Article

# Study of Photovoltaic Double-Skin Façade Windows in Passenger Ships

Song Lv <sup>1,2,3</sup> and Yin Lai <sup>1,2,\*</sup>

<sup>1</sup> Key Laboratory of High Performance Ship Technology, Wuhan University of Technology, Ministry of Education, Wuhan 430063, China

<sup>2</sup> School of Naval Architecture, Ocean and Energy Power Engineering, Wuhan University of Technology, Wuhan 430063, China

<sup>3</sup> School of Materials Science and Engineering, Wuhan University of Technology, Wuhan 430063, China

\* Correspondence: lycqy@whut.edu.cn; Tel.: +86-183-5539-8515

**Abstract:** The ship-mounted photovoltaic (PV) system was an approach to solve the problem of pollution caused by excessive energy consumption during navigation. However, PV systems used on ships faced problems such as small installation areas, which prevented PV power generation from being utilized on a large scale. This article proposes a space-saving photovoltaic double-skin façade (PV-DSF) window system, which could be used in conjunction with ships to address the insufficient ship-mounted photovoltaics. In this paper, we propose a space-saving photovoltaic double-skinned façade (PV-DSF) window system that could be used in conjunction with a ship to solve the problem of insufficient space for onboard photovoltaics. According to the working principle of the system, we established a mathematical model corresponding to the actual heat transfer process and, at the same time built up a corresponding experimental test rig for thermoelectric performance measurement, and verified the accuracy of the proposed mathematical model based on the experimental results. Finally, the effect of different parameters on the performance of the system and the energy performance of the system on board the ship was discussed using a mathematical model. The simulation data showed that the increase of solar radiation intensity, wind speed, and PV coverage had a positive effect on the system's power generation, while the ambient temperature had a negative effect. The system, in combination with a passenger ship, was able to provide 53.2 kWh of annual electricity generation and reduced CO<sub>2</sub> emissions by 17 kg.

**Keywords:** ship-mounted photovoltaic; photovoltaic double-skin façade; thermal performance; power performance



**Citation:** Lv, S.; Lai, Y. Study of Photovoltaic Double-Skin Façade Windows in Passenger Ships. *Sustainability* **2024**, *16*, 3724. <https://doi.org/10.3390/su16093724>

Received: 21 March 2024

Revised: 23 April 2024

Accepted: 24 April 2024

Published: 29 April 2024



**Copyright:** © 2024 by the authors. Licensee MDPI, Basel, Switzerland. This article is an open access article distributed under the terms and conditions of the Creative Commons Attribution (CC BY) license (<https://creativecommons.org/licenses/by/4.0/>).

## 1. Introduction

When ships were sailing or moored on the water for long periods of time, the hull and superstructure were exposed to direct sunlight for long periods of time, while the ship's power electromechanical equipment and personnel were also generating a lot of heat, leading to an increase in the internal temperature of the ship. Therefore, the ship's HVAC (Heating, ventilation, and air conditioning) equipment was an important part of its infrastructure. However, the energy consumption of HVAC equipment was huge, and about 30% of the total electricity consumption of large cruise ships was from HVAC [1]. At present, ships are mainly supplied with energy from fossil fuels [2], which could consume fuels dramatically, increase economic costs, and pollute the environment. According to the International Maritime Organization (IMO), more than 27,000 transport vessels worldwide consumed more than 200 million tons of fuel, and total shipping emissions were about 1 billion tons of CO<sub>2</sub> per year, which was contrary to its initial strategy to reduce greenhouse gas emissions from ships [3]. Due to the increasingly serious problem of ship emissions, energy-efficient emission reduction technologies for the shipping industry have attracted great attention from the international community [4], and the search for new

alternative energy sources has become a pressing issue. Solar radiation, as a clean new energy with huge reserves [5], does not pollute the environment and has the advantage of being inexhaustible and renewable compared to conventional fuel. Hence, if the advantages brought by solar radiation energy could be utilized, it would help ships accomplish the goal of energy-saving navigation and contribute to the fight against environmental pollution [6].

The emergence of photovoltaic cells that could convert collected solar radiation into usable electrical energy [7] and installing PV systems on ships had proved to be a viable means to share some of the power generation tasks of ship engines and reduce energy consumption and pollutant emissions of ships [8], which had a broad research prospect. For example, Lan et al. [9] studied a hydroelectric power system. A method was proposed that enabled the optimum sizing of PV/diesel/battery in hydroelectric power systems, effectively reducing total costs and pollutant emissions. Tang [10] combined ocean-going ships with large-scale PV systems and proposed a new ship power system structure and controlling methods. The result showed that the proposed structure and methods could operate safely and effectively under complex environmental conditions. Zhang et al. [11] focused on some relevant marine environmental factors affecting photovoltaic cells. The results showed that salt spray had an unfavorable effect on photovoltaic cells and reduced their power generation, while seawater would affect the opposite result. Ghenai et al. [12] simulated and optimized a three-in-one (including photovoltaic) energy power system and studied its system performance at a deeper level. It was found that the system provided a 13.83% renewable energy penetration and a 9.84% reduction in pollutant gas and related emissions compared to a diesel engine system. Kurniawan et al. [13] conducted an in-depth study on the placement angle of photovoltaic cells on ships. It was found that the placement angle of PV cells had a relevant influence on their efficiency, and the optimal angle for different sailing cycles was calculated. Karatug et al. [14] designed a PV system for a large ship to provide a portion of the energy supply and conducted a comparative study with a ship without PV. The results showed that ships with PV systems used 7.38% less fuel, which was a significant effect. Wen et al. [15] used mathematical calculations to model and calculate the whole ship photovoltaic system. The optimal coupling of different parts was obtained using numerical simulation to obtain the best efficiency.

From the above research into the use of PV cells in combination with ships, a number of drawbacks have been identified with current PV ship systems. Firstly, most ships were compact and had limited deck space, while the installation of PV cells required more space [16], which resulted in ships not being able to provide enough space for the installation of PV cells, and with the average nominal power of modern crystalline silicon solar cells today typically ranging from 150 W to 300 W, the limited deck space posed a constraint on the total amount of PV power generated with today's lower PV efficiencies. Secondly, when the ship was at sea, it was affected by the marine climate, such as salt spray, which resulted in low solar irradiation, which meant that the PV cells had low power generation performance and could not be used as a primary energy source, but only treated as a secondary energy source. Therefore, we needed to find a new technology for ships and combine it with photovoltaics to solve these problems.

Photovoltaic (PV) modules, in combination with conventional glass windows, are receiving increasing attention from scholars as a new way of utilizing solar energy, capable of controlling radiant heat transfer and converting solar radiation hitting the surface of the window into electrical energy [17]. Meanwhile, double skin façade (DSF) can also be used as an energy-saving building design [18]. There is no doubt that utilizing the PV modules in combination with the DSF (PV-DSF) will bring better results. Han et al. [19] conducted an experimental study on conventional glass windows and new photovoltaic double-ventilated windows. The study shows that under the same environment, photovoltaic double ventilated window has obvious advantages over traditional glass windows and can effectively reduce the indoor temperature, with a difference of 5 °C between the two. Yoon et al. [20] specifically investigated the thermal performance of different double-pane windows. Based on the results of the year-round experiments, it was found that both

in summer and winter, thanks to the thermal radiation performance of double-paned PV windows, they had better temperature performance than double-paned regular windows, which could lead to better thermal comfort. Olivieri et al. [21,22] used mathematical simulations to investigate different factors affecting the efficiency of PV windows in combination with the use of buildings, such as window-to-wall ratio and light transmission ratios. Chae et al. [23] investigated the difference between photovoltaic windows and ordinary windows under various environmental conditions. According to the simulation results, the PV system performed better, with good energy saving and emission reduction regardless of which environment it was in. Peng et al. [24] modeled the performance of ventilated double-skin PV windows in mathematical computing software for a specific climate. The calculation results showed that the ventilated double-skin PV window had a good energy-saving effect compared with double-skin ordinary glass windows and could bear 50% of the electricity consumption of the building. Elarga et al. [25] discussed the combined use of PV systems and DSF buildings and used TRNSYS 16.1 software for dynamic numerical simulation. The simulation calculated that a ventilated double PV façade could effectively reduce the electricity use of a building during the hot and dry European summer due to the power generation effect of the PV modules. Wang et al. [26] employed a novel CdTe cell used in conjunction with a double-layer ventilated window, and its actual performance was measured using experimental and simulation means. It was obtained that the system had good electrical performance in both winter and summer and was able to provide the building with 205.76 and 333.09 kWh of electricity, respectively.

In light of the above discussions, the PV-DSF system had promising application prospects and could realize energy saving and emission reduction to a certain extent. In such a way as to address the issue of excessive energy consumption during navigation, we proposed a PV-DSF window system that combined with ships. Firstly, the energy balance equation was established based on the system's actual heat transfer process. Then, a simple test rig was set up to replace the PV-DSF system and utilized in conjunction with the ship to measure the specific thermo-electric performance of the system in the external environment, and then the experimental results were used to validate the previous mathematical equations. Finally, based on the previous step, different factors affecting the thermoelectric performance of the PV-DSF system were investigated using simulations, and the possibility of PV-DSF application on ships was discussed. We provided guidance for achieving truly green and energy-efficient navigation for ships.

## 2. Theoretical Models

In this part, a mathematical model was developed to simulate the thermoelectric performance of the system under ideal conditions. The mathematical model incorporated the heat transfer process for each component, including the PV glass, air channel, and glass.

Considering the complexity of the mathematical model, in order to facilitate the simulation calculations, some hypotheses were made about the proposed mathematical model [26–28]:

- (1) Only the change in temperature of each part of the vertical direction was considered.
- (2) Heat transfer between the window section and the frame was ignored.
- (3) None of the thermal parameters in the system varied with temperature.
- (4) Solar radiation did not enter the room through the PV-DSF model.
- (5) The electrical efficiency of photovoltaic cells did not decrease when the temperature rose.
- (6) Physical properties were steady.

### 2.1. Solar Radiation

Specific data on solar radiation could be obtained from meteorological data, generally only horizontal solar radiation data, including three parts, namely beam radiation,  $I_b$ , diffuse reflection  $I_d$  and reflected radiation  $I_r$ .

The solar radiation received by arbitrary angle was [29]:

$$I = I_b R_b + 0.5 I_d (1 + \cos \beta) + 0.5 \zeta (I_b + I_d) (1 - \cos \beta) \quad (1)$$

$$R_b = \frac{\cos \theta}{\cos \theta_z} \quad (2)$$

$$\cos \theta_z = \cos \phi \cos \delta \cos \omega + \sin \phi \sin \delta \quad (3)$$

where  $\beta$  was inclined angle,  $\zeta$  was reflectance coefficient,  $\theta$  was incidence angle,  $\theta_z$  was the zenith angle.

## 2.2. PV Glass

The main energy transfers of PV glass were: heat storage, conduction, convection and radiation with the outdoor environment, radiation with inner glass, convection with the air in the channel, absorption of solar radiation, and electrical output. The energy balance equation as followed:

$$d_{pv} \rho_{pv} c_{pv} \frac{\partial T_{pv}}{\partial t} = d_{pv} \lambda_{pv} \frac{\partial^2 T_{pv}}{\partial y^2} + h_{amb} (T_{amb} - T_{pv}) + h_{rad} (T_{sky} - T_{pv}) + h_g (T_g - T_{pv}) + h_{air} (T_{air} - T_{pv}) + I \alpha_{pv} - E \quad (4)$$

where  $d_{pv}$ ,  $\rho_{pv}$ ,  $c_{pv}$  and  $T_{pv}$  were the thickness, density, specific heat and temperature of the PV glass, respectively.  $\lambda_{pv}$  was the thermal conductivity.  $I$  and  $\alpha_{pv}$  were the solar radiation intensity and the absorptivity of PV glass.  $T_{amb}$  and  $T_{sky}$  were the temperature of outdoor environment and the sky respectively. And  $T_{sky}$  was shown as [30]:

$$T_{sky} = 0.0552 T_{amb}^{1.5} \quad (5)$$

$h_{amb}$ ,  $h_{rad}$ ,  $h_g$  and  $h_{air}$  were the convection and radiation heat transfer coefficient between PV glass and outdoor air, the radiative heat transfer coefficient between PV glass and glass, the convective heat transfer coefficient between PV glass and air, and defined as [29,31,32]:

$$h_{amb} = 5.6 + 3.9V \quad (6)$$

$$h_{rad} = \varepsilon_{pv} \sigma (T_{sky}^2 + T_{pv}^2) (T_{sky} + T_{pv}) \quad (7)$$

$$h_g = \frac{\sigma (T_{pv}^2 + T_g^2) (T_{pv} + T_g)}{\frac{1}{\varepsilon_{pv}} + \frac{1}{\varepsilon_g} - 1} \quad (8)$$

where  $V$  was the ambient wind speed.  $\sigma$  was the Stefan-Boltzmann's constant.  $\varepsilon_{pv}$  and  $\varepsilon_g$  were the emissivity coefficients of the PV glass and glass, respectively.

$h_{air}$  was the convective heat transfer coefficient between two panes and air in the channel, which could be calculated as [32,33].

When the vents were opening,

$$h_{air} = 5.6 + 3.9V_{air} \quad (9)$$

When the vents were closing,

$$h_{air} = \frac{Nu \cdot k_{air}}{L} \quad (10)$$

where  $Nu$  was the Nusselt number.  $k_{air}$  was the air thermal conductivity.  $L$  was the depth of the air channel.

$E$  was the electric output power by PV cells, and it was shown as [34]:

$$E = I \zeta \tau \eta [1 - \psi (T_{pv} - 25)] \quad (11)$$

where  $\zeta$  was the PV coverage ratio.  $\tau$  was the transmittance of the outer glass layer of PV glass.  $\eta$  was the electrical efficiency of the PV under standard conditions.  $\psi$  was the temperature coefficient.

### 2.3. Air Channel

The main energy transfers of the air channel were heat storage, convection with PV glass and glass, and airflow along the vertical direction. The energy balance equation is as follows:

$$L\rho_{air}c_{air}\frac{\partial T_{air}}{\partial t} = h_{air}(T_{pv} - T_{air}) + h_{air}(T_g - T_{air}) - L\rho_{air}V_{air}c_{air}\frac{\partial T_{air}}{\partial y} \quad (12)$$

where  $\rho_{air}$ ,  $c_{air}$ , and  $T_{air}$  were the density, heat capacity and temperature of the air channel, respectively.  $V_{air}$  was the air velocity in the channel, and defined as [33,35]:

$$V_{air} = \sqrt{\frac{g\bar{\beta}(T_{out} - T_{in})H}{C_f\frac{H}{D} + C_{in}\left(\frac{A}{A_{in}}\right)^2 + C_{out}\left(\frac{A}{A_{out}}\right)^2}} \quad (13)$$

where  $g$  was the gravity constant.  $\bar{\beta}$  was the volumetric expansion coefficient of the air.  $T_{out}$  and  $T_{in}$  were the air temperature of the outlet and inlet of the air channel, respectively.  $H$  and  $D$  were the height and the hydraulic diameter of the air channel, respectively.  $A$ ,  $A_{in}$ , and  $A_{out}$  were the cross-sectional areas of the air channel, the cross-sectional areas of the inlet and outlet, respectively.  $C_f$ ,  $C_{in}$ , and  $C_{out}$  were the friction factor along the channel, the loss coefficients of the inlet and the outlet, respectively.

### 2.4. Glass

The main energy transfers of glass were: heat storage, conduction, convection with the air in the channel, radiation with outer PV glass, convection with indoor air, and absorption of solar radiation. The energy balance equation is as follows:

$$d_g\rho_gc_g\frac{\partial T_g}{\partial t} = d_g\lambda_g\frac{\partial^2 T_g}{\partial y^2} + h_{air}(T_{air} - T_g) + h_g(T_{pv} - T_g) + h_{room}(T_{room} - T_g) + I\tau_{pv}\alpha_g \quad (14)$$

where  $d_g$ ,  $\rho_g$ ,  $c_g$ , and  $T_g$  were the thickness, density, specific heat, and temperature of the glass, respectively.  $\lambda_g$  was the thermal conductivity.  $\tau_{pv}$  and  $\alpha_g$  were the transmittance of PV glass. and the absorptivity of glass.  $T_{room}$  was the temperature of indoor air  $h_{room}$  was the convective heat transfer coefficient between the glass and indoor air, it was shown as [36]:

$$h_{room} = 2.03|T_g - T_{room}|^{1/3} \quad (15)$$

## 3. Experimental Setup

From outdoor to indoor, the window system consisted of PV glass, vents, air channels, and glass. Figure 1 shows the exterior view of the experimental system. The outer layer was the PV glass consisting of CdTe and ultra-white float glass, 7 mm thick. Its electrical performance parameters under STC (standard testing condition) are listed in Table 1. The inner layer of the glass was plain clear glass, 5 mm thick. A 100 mm deep air channel existed between the two layers mentioned above. Vents were provided above and below the outer layer. The thermal pressure ordered the air to enter through the lower vent and exit through the upper vent. This airflow was able to carry away a certain part of the heat generated by the PV glass, increasing the efficiency of the PV. The size of the test rig was 800 mm in length, 1800 mm in width, and 800 mm in height. The overall frame of the test rig was made of stainless steel, except for the side with the installed window, which is made of aluminum foil polyurethane insulation board and reflective film. The size of each vent was 600 mm in width and 150 mm in height.

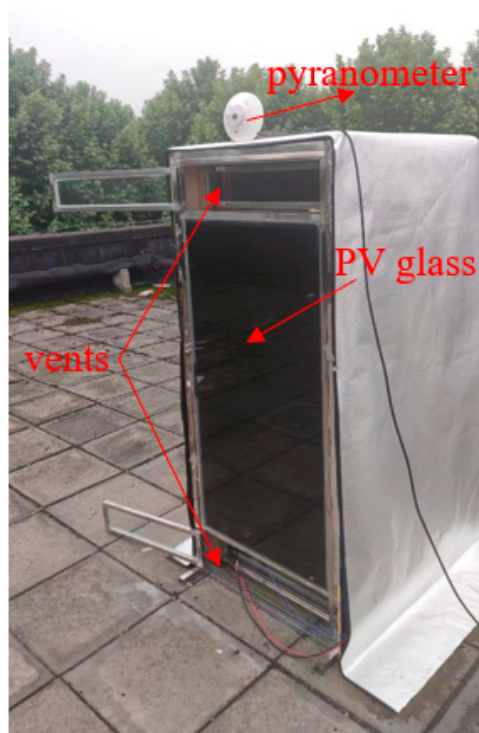


**Figure 1.** The exterior view of the experiment system.

**Table 1.** Electrical parameters of CdTe PV module.

Parameters	Values
Maximum power ( $E_m$ )	76 (W)
Open circuit voltage ( $V_{oc}$ )	122.5 (V)
Short circuit current ( $I_{sc}$ )	0.98 (A)
Voltage at maximum power point ( $V_{mp}$ )	89.7 (V)
Current at maximum power point ( $I_{mp}$ )	0.85 (A)
PV module efficiency	10.56%
Temperature coefficient of $V_{oc}$	$-0.321\%/^{\circ}\text{C}$
Temperature coefficient of $I_{sc}$	$0.060\%/^{\circ}\text{C}$
Temperature coefficient of $E_m$	$-0.214\%/^{\circ}\text{C}$
PV coverage ratio	80%

All temperature measurement points during the experimental measurements were made by type K thermocouples, including the ambient temperature, the temperature of each part of the window, and the room temperature. The accuracy of the thermocouple was  $\pm 0.5^{\circ}\text{C}$ . Daytime solar radiation intensity measurements were obtained from a pyranometer model TBQ-2, which mainly measured the visible light band from 280 to 3000 nm with a sensitivity of  $10.197 \mu\text{V}/(\text{W}\cdot\text{m}^{-2})$ . The accuracy of the pyranometer was  $\pm 2\%$ . Temperature measurements were exported using a K-type thermocouple connected to a LR8402-21 type data collector from HIOKI (Nagano, Japan), and data were recorded for 1 s. The power of the PV module is measured by a power meter with an accuracy of  $\pm 1\%$ . The specific experimental measurement schematic is shown in Figure 2.

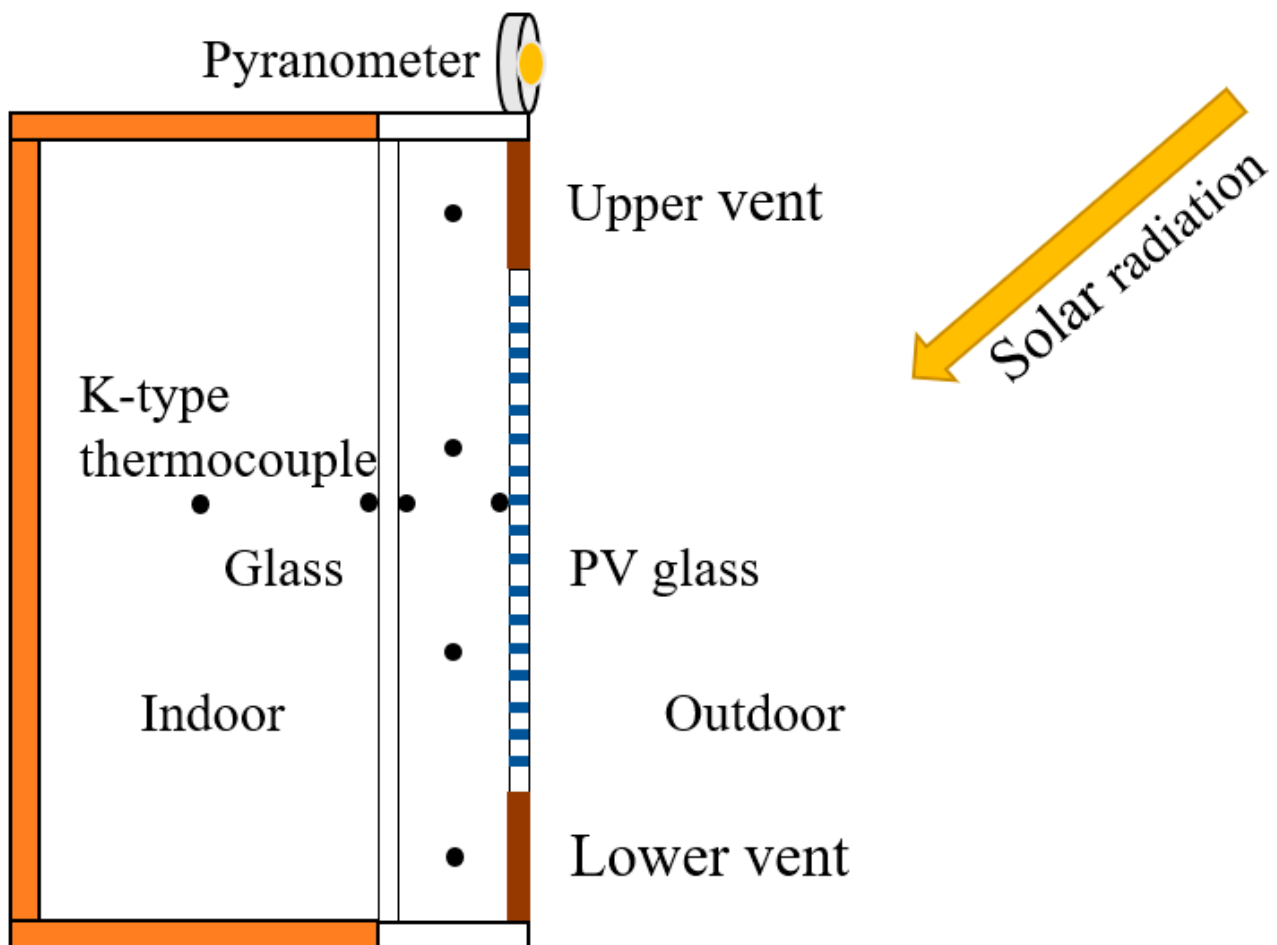


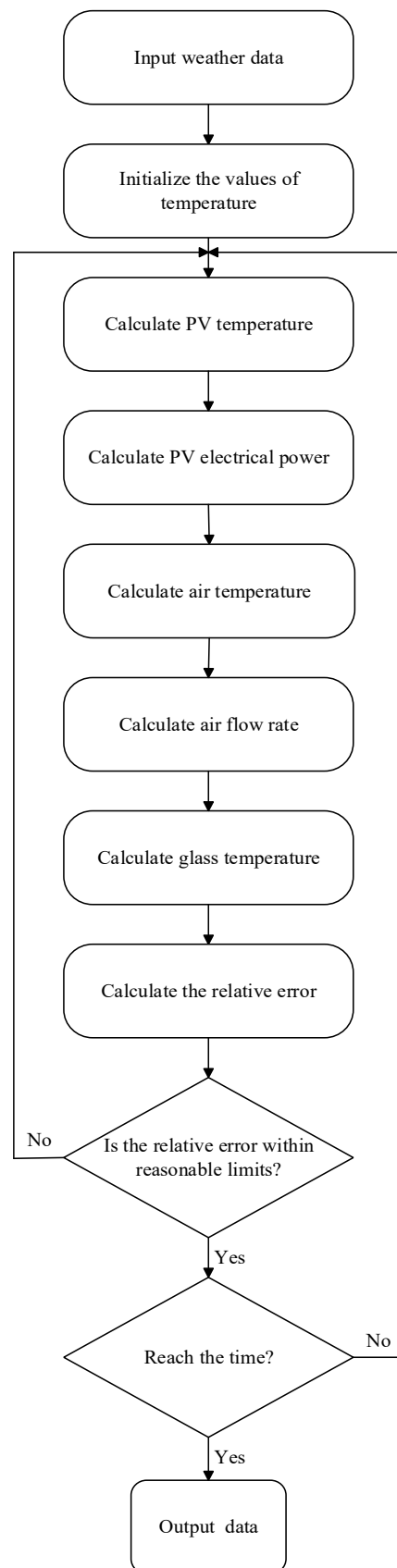
**Figure 2.** The specific experimental measurement schematic.

We installed the test rig in Wuhan, China (30° N, 114° E) for measurements in an outdoor environment. The test rig was placed on an empty roof in order to achieve unobstructed sunlight for better experimental purposes.

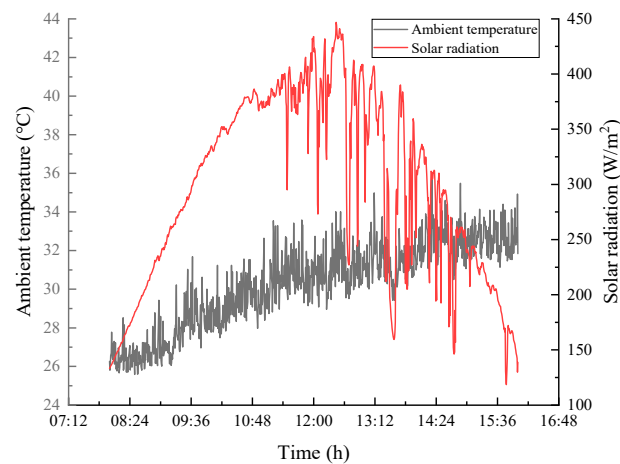
#### 4. Model Validation

In order to solve the heat transfer energy balance equations for each of the above components, the corresponding computational programs were written in MATLAB R2019b software. The method used for the computational procedure was the finite difference method. The simulation had a time step of 1 s, which means that the corresponding time step for the weather data was also 1 s. The computational flowchart for each part of the system was shown in Figure 3.

In order to ensure that the proposed PV-DSF model had sufficient computational accuracy during the daytime, the period from 8 A.M. to 4 P.M. of the day was chosen here. Figure 4 shows the specific external environmental data on the day of our measurements. The overall trend of solar radiation during the day is to increase and then decrease, with a maximum value of around 450 W/m<sup>2</sup>. However, due to cloud cover, the solar radiation fluctuated very sharply around 12 noon. The ambient temperature rose gradually from 24 °C to 34 °C, then dropped slightly and finally stabilized.

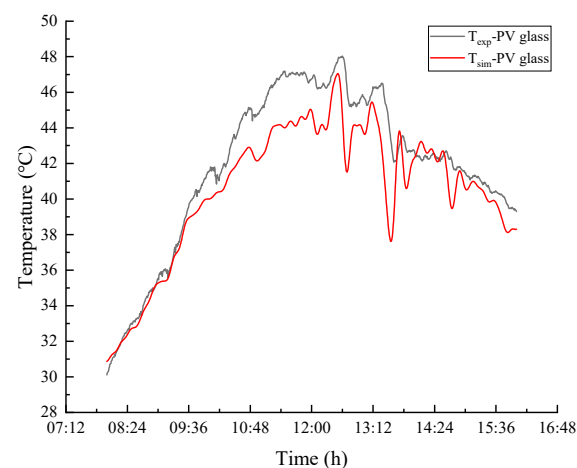


**Figure 3.** The computational flowchart of the system.



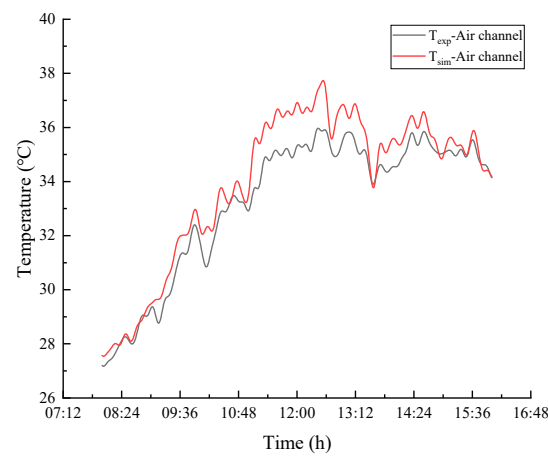
**Figure 4.** The ambient temperature and solar radiation during the experiment.

Figure 5a–c shows the experimentally measured temperature data and the corresponding simulated data, which could clearly be seen to be close to each other without excessive differences. The temperature of the PV glass in the outer layer varied with the solar radiation, having the same trend. The temperature of the PV glass obtained from the simulation would also change significantly when there were sharp fluctuations in solar radiation near noon, but the experimentally measured PV glass temperature would only have a smaller change, not as drastic as the change in the simulation. This was because this part of the solar radiation changed too drastically in the simulation, but the actual measurement did not have too much change in temperature due to the rapid change in solar radiation, so it leads to a certain error. The temperature trends in the air channel and glass were also similar to the trend in solar radiation. The maximum experimental temperatures for PV glass, air channel, and glass were about 48 °C, 36 °C, and 39 °C, respectively. It can be seen from Figure 5d that the experimental power data and the corresponding data were obtained by simulation. It was not difficult to see that the maximum experimental power generation point appeared when the solar radiation was the largest, about 24 W. The overall trend in power is generally consistent with solar radiation, and the trend of the experimental power and the simulated power were also in general agreement.

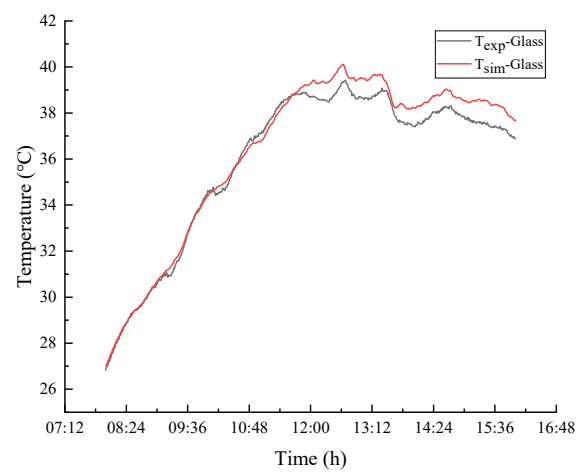


**(a)** Temperature of PV glass

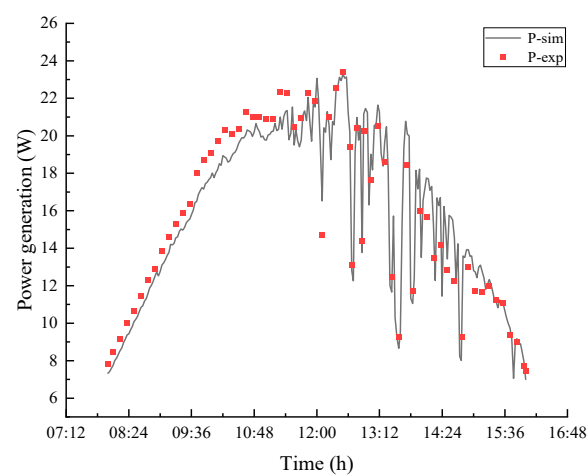
**Figure 5.** Cont.



(b) Temperature of air channel



(c) Temperature of glass



(d) Power generation of PV glass

**Figure 5.** Experimental and simulated comparisons of temperature and power of each part of the system.

In order to ensure the reliability of the mathematical model, the root mean square deviation (RMSD) calculation was used here for validation, which was given as [37]:

$$RMSD = \sqrt{\frac{\sum [(x_{sim} - x_{exp}) / x_{exp}]^2}{n}} \times 100\% \quad (16)$$

where  $x_{sim}$  and  $x_{exp}$  were the simulation and experimental results and  $n$  was the total number of data points.

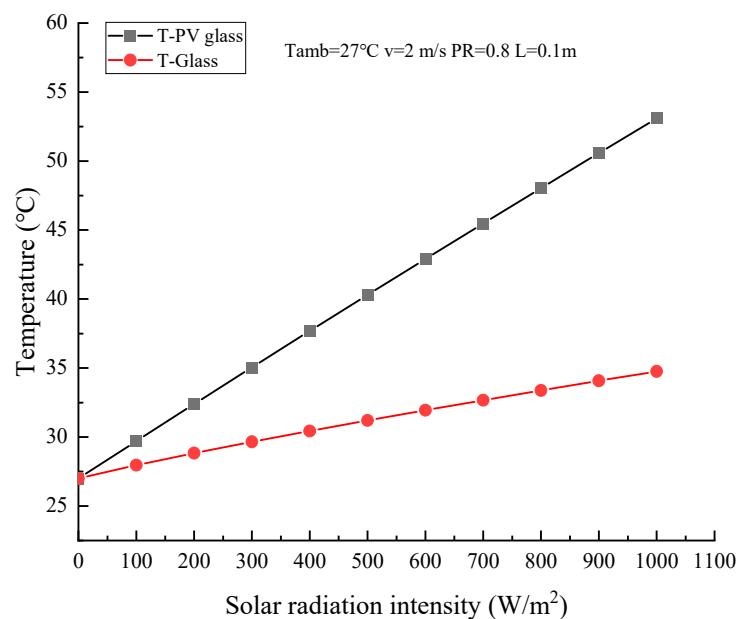
The root mean square deviation between the experimental and simulated data was 4.4% for PV glass, 2.5% for air channels, 1.5% for glass, and 7.2% for power. Therefore, based on the error results, the proposed theoretical mathematical model was sufficiently accurate to simulate the real heat transfer in the actual PV-DSF process.

## 5. Results and Discussion

Changes in the marine environment had a non-negligible impact on the overall performance of the system. For example, drastic changes in the surrounding environment could affect convection and radiation in the system, which could cause heat loss. In addition, parameters within the model, such as PV coverage ratio, could also have an impact. Therefore, on the basis of the previously validated mathematical models, the main factors affecting the performance of the proposed PV-DSF model, such as solar radiation intensity, ambient temperature, wind speed, and PV coverage ratio, were discussed. Finally, an energy analysis of the system in conjunction with a passenger ship was made.

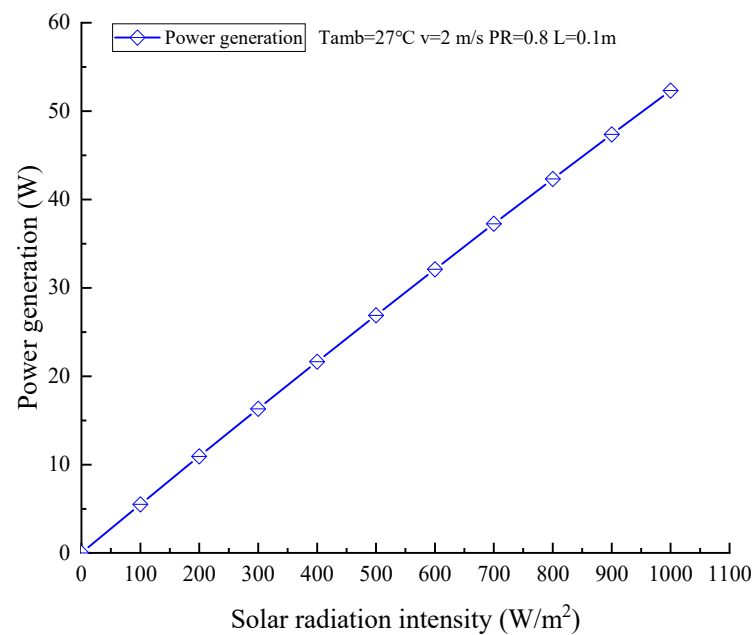
### 5.1. Solar Radiation Intensity

Daytime solar radiation was the most important energy input to the PV-DSF model and had a substantial impact on the model's overall performance due to its high energy density. The temperature change of the inner glass and the variations in power generation and temperature of the outer PV glass both demonstrated this role. Figure 6a,b showed the temperature and power generation of the PV-DSF model for different solar radiation densities in an environment where all other conditions were equal.



(a) Temperature of the outer PV glass and the inner glass

Figure 6. Cont.



(b) Power generation of PV glass

**Figure 6.** Temperature and power of the PV-DSF model at different solar radiation intensities.

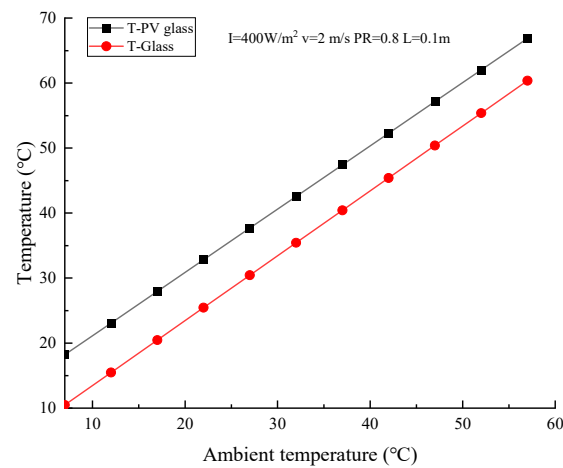
For the proposed PV-DSF window model, it was observed from Figure 6a that as the solar radiation intensity increased sequentially from 0 to 1000 W/m<sup>2</sup>, the temperature of the inner and outer layers and the PV power generation would also increase accordingly. The PV power generation had the largest upward trend, and the upward trend of the outer layer temperature was greater than the inner layer temperature. Specifically, the temperature of the outer PV glass increased from about 27 to 53 °C, the inner glass increased from about 27 to 35 °C, and the PV glass power generation increased from about 0 to 52 W.

The reason for this was that when solar radiation hits the outer glass, most of the energy would be absorbed by the outer layer due to the absorbent nature of the photovoltaic glass, with a small percentage passing through the outer layer to the inner layer. From the above results, it could be concluded that the solar radiation intensity as the main energy input had a great influence on the temperature and power generation of the whole system.

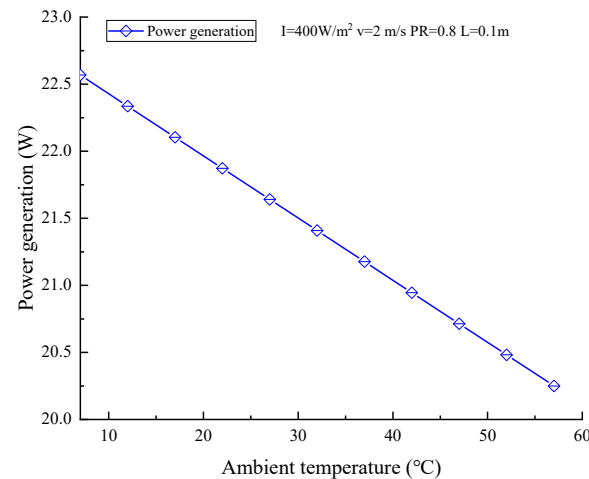
### 5.2. Ambient Temperature

For the PV-DSF system that was exposed to the external environment for a long time, the ambient temperature would be one of the most important performance influences that could not be ignored. A rise or fall in ambient temperature would inevitably cause changes in the heat exchange with the system. Figure 7a,b show the temperature and power generation of the PV-DSF model for different outside ambient temperatures in an otherwise identical environment.

From the simulation results in Figure 7a, it could be clearly observed that there was a positive correlation between the temperature of the inner and outer glass layers and the ambient temperature. As the ambient temperature gradually increased, the heat exchange between the outer PV glass and the atmosphere increased significantly, and the temperature of the PV glass also rose. Meanwhile, the temperature of the inner glass rises as the temperature of the outer PV glass rises due to the heat transfer within the system. Then, the power generation is shown in Figure 7b. Specifically, the ambient temperature rises from 7 to 57 °C, the temperature of the outer glass rises from about 18 to 67 °C, the temperature of the inner glass rises from about 10 to 60 °C, and the power generation from about 22.5 to 20W.



(a) Temperature of the outer PV glass and the inner glass



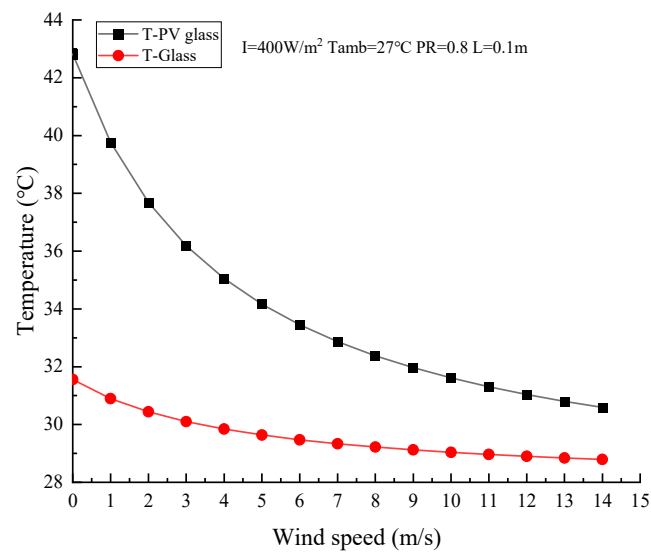
(b) Power generation of PV glass

**Figure 7.** Temperature and power of the PV-DSF model at different ambient temperatures.

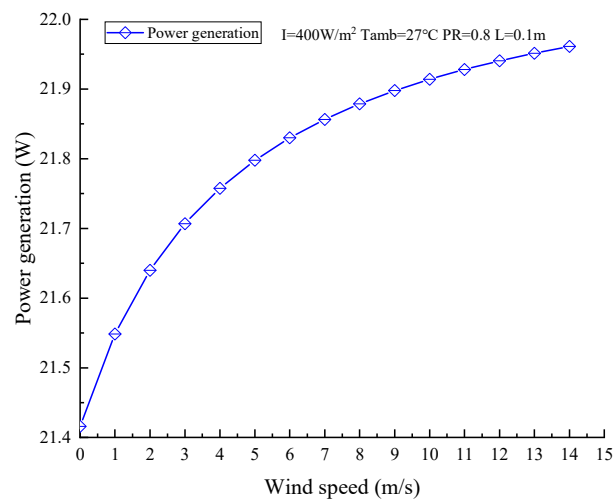
### 5.3. Wind Speed

The convective heat transfer coefficient between the outer glass and the external environment was mostly influenced by wind speed in the PV-DSF model, and there was a positive correlation between the two. As a result, it was essential to research how the model would function at various wind speeds. Figure 8a,b shows the temperature and power generation of the PV-DSF model for different wind speeds in the exact same environment.

According to the results in Figure 8a, the increasing outside wind speed had a negative effect on the temperature of both the inner and outer glass. For the outer PV glass, the temperature change is greater as the wind speed increases from 0 to 14 m/s, changing from about 43 to 30 °C. For the inner glass, the temperature changed little during the wind speed change from 0 to 14 m/s, from about 31 to 29 °C. The reason for this was that the ambient wind speed had a direct effect on the outer glass, and therefore, the temperature of the outer glass varied more. The inner glass temperature was affected by the outer glass temperature, so only a slight change occurred. Due to the relatively small temperature coefficient of the PV cell, the change in power generation is small. The trend of change in power generation was shown in Figure 8b and was consistent with the trend of change in temperature of the outer glass, with a range of about 21.4 to 22 W.



(a) Temperature of the outer PV glass and the inner glass



(b) Power generation of PV glass

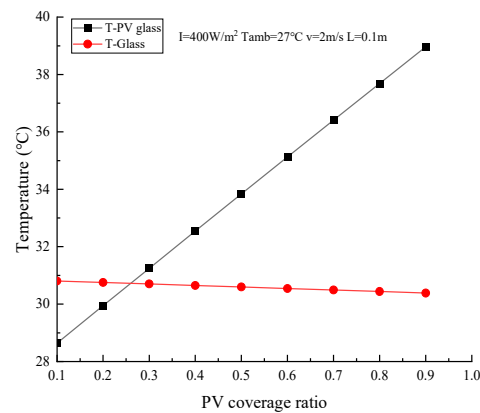
**Figure 8.** Temperature and power of the PV-DSF model at different wind speeds.

#### 5.4. PV Coverage Ratio

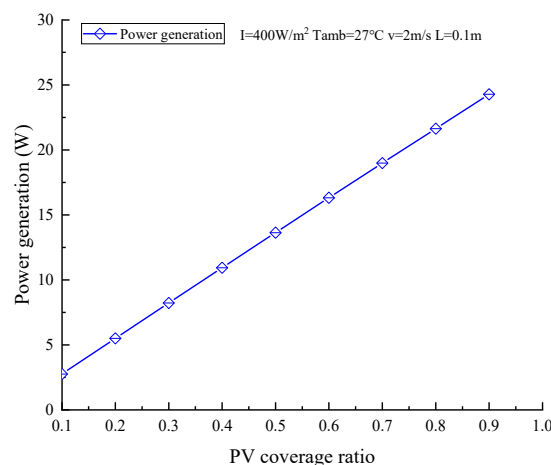
For the PV-DSF model, the PV coverage ratio had an important relationship to power generation, with PV module power increasing as PV coverage increased. Consequently, it was necessary to study the performance of the system under different PV coverage ratios. Figure 9a,b shows the temperature and power generation of the PV-DSF model for different PV coverage ratios in the exact same environment.

It was clear from Figure 9a that the temperature of both the inner and outer glass increases as the PV coverage increases. The difference here was that the temperature of the outer PV glass rose significantly, from about 29 to 40 °C, while the inner glass temperature changed slightly, from about 31 to 30 °C. The reason for this was that the absorption rate of the outer PV glass was much greater than that of the inner glass. When the PV coverage was very small, most of the solar radiation shone through the outer glass to the inner glass, but only a small part was absorbed by the inner glass, and when the PV coverage was large,

the solar radiation shone through the outer glass and was mostly absorbed. The trend in power generation is shown in Figure 9b, with a clear increase in power as PV coverage rose, ranging from about 3 to 24 W.



(a) Temperature of the outer PV glass and the inner glass



(b) Power generation of PV glass

**Figure 9.** Temperature and power of PV-DSF models at different PV coverage ratios.

### 5.5. Energy Analysis

In the previous section, we analyzed the effects of the environmental factors on the water surface and the system parameters on the performance of the PV-DSF system. In order to better investigate the performance of the system in combination with the ship, in this section, we will investigate the integration of the system on board a passenger ship named “Wind Solar Show” by our university. Figure 10 reflects the exterior view of the passenger ship.

There were four locations in the ship’s cabin where the PV-DSF system could be installed, namely the front, rear, right, and left windows, but the system was not fitted to the front window in view of the fact that they would adversely affect the transparency required for driving. Table 2 shows the size of the PV-DSF system area in each part of the ship. The orientation of this PV-DSF system at different positions was as follows: right window facing west with  $90^\circ$  azimuth and  $90^\circ$  inclination, left window facing east with  $-90^\circ$  azimuth and  $90^\circ$  inclination, and rear window facing north with  $180^\circ$  azimuth and  $90^\circ$  inclination. Figure 11 shows the monthly solar radiation and monthly mean temperature data obtained from the Meteonorm 8 software for different location orientations. The total

amount of solar radiation received by the left and right windows are similar, while the rear window received the least amount of solar radiation due to its north orientation.



Figure 10. Exterior view of the passenger ship “Wind Solar Show”.

Table 2. Area of PV-DSF system installed in each section.

Position	Values
Right window	0.45 (m <sup>2</sup> )
Left window	0.45 (m <sup>2</sup> )
Rear window	0.2 (m <sup>2</sup> )

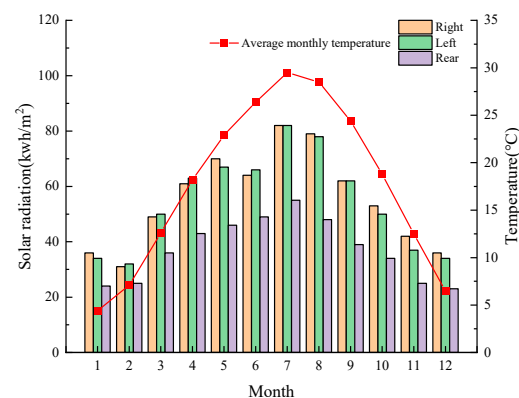
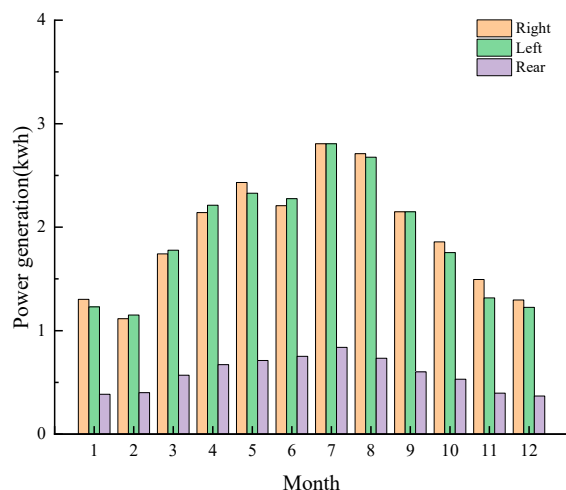


Figure 11. Total monthly solar radiation received by different parts of the system and average temperatures.

The magnitude of the electrical power generated by the PV-DSF system in three directions, the right window, the left window, and the rear window, is shown in Figure 12. As could be seen from the data in the figure, the rear window generated the least amount of electricity compared to the right and left windows due to the fact that this part of the rear window had the smallest area of the PV-DSF system installed, as well as the fact that it received the least amount of total solar radiation, as mentioned earlier. The maximum power generation of the system at all three locations occurred in July. The total annual power generation from the right, left, and rear windows was about 23.3 kwh, 22.9 kwh, and 7 kwh, respectively, and the total power generation from the PV-DSF system integrated into the whole passenger ship was 53.2 kwh. Based on the standard coal equivalent conversion, the total annual power generation of the system was able to replace the electricity generated by 6.5 kg of coal, which reduced the CO<sub>2</sub> pollution emission by about 17 kg.



**Figure 12.** The power output of the system at different positions.

## 6. Conclusions

In summary, we used photovoltaic windows to replace traditional windows, utilizing daylight through photovoltaic power generation technology. At the same time, it could also save part of the energy during ship navigation. Subsequently, we established a mathematical model of the system based on the actual heat transfer process and discussed the various factors affecting the system performance as well as the related energy analysis in conjunction with the experiments. The specific conclusions were as follows:

- (1) Solar radiation intensity, as the main input energy source, played a decisive role in the thermoelectric performance of the whole PV-DSF model. This was manifested by the positive correlation trend between solar radiation intensity and temperature and power generation.
- (2) Ambient temperature was an important influence on the heat exchange between the system and its surroundings. When the ambient temperature increased, the overall temperature of the PV-DSF model also increased significantly because of the heat exchange. However, as the temperature of the PV glass increased, the power generation tended to decrease, from about 22.5 W to 20 W, which was a decrease of 11%.
- (3) Wind speed had a negatively correlated effect on the thermal performance of the PV-DSF model. The wind speed had a strong effect on the temperature of the outer glass, while it had little effect on the inner glass. As wind speed continued to increase, the model's power generation increased slightly, from about 21.4 W to 22 W, an increase of about 3%. It was worth noting that there would be an upper limit to the effect of wind speed on the overall performance of the model, as evidenced by the fact that the performance of the system changed less and less as the wind speed continued to increase.
- (4) There was a direct link between the PV coverage and the electrical performance of the PV-DSF model. As the PV coverage increased, the power generation also increased from about 3 W to 24 W, an increase of 700%. The thermal impact on the outer glass layer was much greater than the inner glass layer due to PV light absorption.
- (5) The PV-DSF system was installed in the ship's right, left and rear windows to provide a total of 53.2 kwh of annual electricity generation and a reduction of 17 kg of CO<sub>2</sub> emissions.

From the above conclusions, it could be obtained that the system had the potential to generate electricity in some ocean special environments (high wind speed), and the energy analysis could also determine that the system had some emission reduction capability. Therefore, our proposed PV-DSF system could be applied to ships. Our future work will

focus on experiments with the system installed on real ships to investigate the actual energy-saving and emission-reduction effects of the system.

**Author Contributions:** Conceptualization, S.L.; Writing—original draft, Y.L. All authors have read and agreed to the published version of the manuscript.

**Funding:** This study was sponsored by the National Natural Science Foundation of China (NSFC 52106268) and the National Natural Science Foundation of Hubei Province, China (No. 2022CFB748).

**Institutional Review Board Statement:** Not applicable.

**Informed Consent Statement:** Not applicable.

**Data Availability Statement:** Data are contained within the article.

**Conflicts of Interest:** The authors declare no conflict of interest.

## Nomenclature

### Symbol

$I$	Solar radiation, $W/m^2$
$\beta$	Inclined angle, $^\circ$
$\zeta$	Reflectance coefficient
$\theta$	Incidence angle, $^\circ$
$\theta_z$	Zenith angle, $^\circ$
$d$	Thickness, m
$\rho$	Density, $kg/m^3$
$c$	Heat capacity, $J/kg \cdot K$
$\lambda$	Heat conductivity, $W/m \cdot K$
$T$	Temperature, $^\circ C$
$\alpha$	Absorptivity
$h$	Convection, $W/m^2 \cdot K$
$V$	Wind speed, m/s
$\varepsilon$	Emissivity
$\sigma$	Stefan-Boltzmann's constant, $W/m^2 \cdot K^4$
$Nu$	Nusselt number
$k$	Conduction, $W/m \cdot K$
$L$	Depth, m
$\zeta$	PV coverage ratio
$\tau$	Transmittance
$\eta$	Electrical efficiency
$\eta$	Electrical efficiency
$\psi$	Temperature coefficient
$g$	Gravity constant, $m/s^2$
$\bar{\beta}$	Volumetric expansion coefficient
$H$	Height, m
$D$	Hydraulic diameter, m
$A$	Area, $m^2$
$C$	Loss coefficient

### Subscripts

$b$	Beam radiation
$d$	Diffuse reflection
$r$	Reflected radiation
$pv$	PV glass
$amb$	Outdoor air
$rad$	Radiation
$g$	Clear glass
$air$	Air in the channel
$out$	Outlet of the air channel
$in$	Inlet of the air channel

$f$  Air channel  
 $room$  Indoor air

## References

- Ivanova, G.; IEEE. Ways to Increase the Efficiency of a Ship Cooling System. In Proceedings of the 13th Electrical Engineering Faculty Conference (BulEF), Varna, Bulgaria, 8–11 September 2021.
- Xie, P.L.; Tan, S.; Guerrero, J.M.; Vasquez, J.C. MPC-informed ECMS based real-time power management strategy for hybrid electric ship. *Energy Rep.* **2021**, *7*, 126–133. [\[CrossRef\]](#)
- Wang, W.; Liu, Y.N.; Zhen, L.; Wang, H. How to Deploy Electric Ships for Green Shipping. *J. Mar. Sci. Eng.* **2022**, *10*, 18. [\[CrossRef\]](#)
- Otsason, R.; Tapaninen, U. Decarbonizing City Water Traffic: Case of Comparing Electric and Diesel-Powered Ferries. *Sustainability* **2023**, *15*, 16170. [\[CrossRef\]](#)
- Ni, J.; Li, J.; An, W.; Zhu, T. Performance analysis of nanofluid-based spectral splitting PV/T system in combined heating and power application. *Appl. Therm. Eng.* **2018**, *129*, 1160–1170. [\[CrossRef\]](#)
- Yigit, K.; Acarkan, B. A new ship energy management algorithm to the smart electricity grid system. *Int. J. Energy Res.* **2018**, *42*, 2741–2756. [\[CrossRef\]](#)
- Lv, S.; Zhang, M.M.; Lai, Y.; Wu, Y.Y.; Deng, J.C.; Guo, Y.; Feng, M.Q.; Shi, G.Q.; Zhang, B.L.; Ren, J.W.; et al. Comparative analysis of photovoltaic thermoelectric systems using different photovoltaic cells. *Appl. Therm. Eng.* **2023**, *235*, 11. [\[CrossRef\]](#)
- Glykas, A.; Papaioannou, G.; Perissakis, S. Application and cost-benefit analysis of solar hybrid power installation on merchant marine vessels. *Ocean Eng.* **2010**, *37*, 592–602. [\[CrossRef\]](#)
- Lan, H.; Wen, S.L.; Hong, Y.Y.; Yu, D.C.; Zhang, L.J. Optimal sizing of hybrid PV/diesel/battery in ship power system. *Appl. Energy* **2015**, *158*, 26–34. [\[CrossRef\]](#)
- Tang, R.L. Large-scale photovoltaic system on green ship and its MPPT controlling. *Sol. Energy* **2017**, *157*, 614–628. [\[CrossRef\]](#)
- Zhang, Y.; Yuan, C.Q. Effects of marine environment on electrical output characteristics of PV module. *J. Renew. Sustain. Energy* **2021**, *13*, 9. [\[CrossRef\]](#)
- Ghenai, C.; Bettayeb, M.; Brdjanin, B.; Hamid, A.K. Hybrid solar PV/PEM fuel Cell/Diesel Generator power system for cruise ship: A case study in Stockholm, Sweden. *Case Stud. Therm. Eng.* **2019**, *14*, 9. [\[CrossRef\]](#)
- Kurniawan, A.; Shintaku, E. Determining the optimal inclination and orientation angles of solar panels installed on ship. *Int. J. Renew. Energy Res.* **2020**, *10*, 45–53.
- Karatug, C.; Durmusoglu, Y. Design of a solar photovoltaic system for a Ro-Ro ship and estimation of performance analysis: A case study. *Sol. Energy* **2020**, *207*, 1259–1268. [\[CrossRef\]](#)
- Wen, S.L.; Lan, H.; Yu, D.C.; Fu, Q.; Hong, Y.Y.; Yu, L.J.; Yang, R.R. Optimal sizing of hybrid energy storage sub-systems in PV/diesel ship power system using frequency analysis. *Energy* **2017**, *140*, 198–208. [\[CrossRef\]](#)
- Sun, Y.W.; Yan, X.P.; Yuan, C.Q.; Tang, X.J.; Malekian, R.; Guo, C.; Li, Z.X. The application of hybrid photovoltaic system on the ocean-going ship: Engineering practice and experimental research. *J. Mar. Eng. Technol.* **2019**, *18*, 56–66. [\[CrossRef\]](#)
- Wang, C.Y.; Uddin, M.M.; Ji, J.; Yu, B.D.; Wang, J. The performance analysis of a double-skin ventilated window integrated with CdTe cells in typical climate regions. *Energy Build.* **2021**, *241*, 17. [\[CrossRef\]](#)
- Zhou, J.; Chen, Y.M. A review on applying ventilated double-skin facade to buildings in hot-summer and cold-winter zone in China. *Renew. Sustain. Energy Rev.* **2010**, *14*, 1321–1328. [\[CrossRef\]](#)
- Han, J.; Lu, L.; Peng, J.Q.; Yang, H.X. Performance of ventilated double-sided PV facade compared with conventional clear glass facade. *Energy Build.* **2013**, *56*, 204–209. [\[CrossRef\]](#)
- Yoon, J.H.; Shim, S.R.; An, Y.S.; Lee, K.H. An experimental study on the annual surface temperature characteristics of amorphous silicon BIPV window. *Energy Build.* **2013**, *62*, 166–175. [\[CrossRef\]](#)
- Olivieri, L.; Caamano-Martin, E.; Moralejo-Vazquez, F.J.; Martin-Chivelet, N.; Olivieri, F.; Neila-Gonzalez, F.J. Energy saving potential of semi-transparent photovoltaic elements for building integration. *Energy* **2014**, *76*, 572–583. [\[CrossRef\]](#)
- Olivieri, L.; Caamano-Martin, E.; Olivieri, F.; Neila, J. Integral energy performance characterization of semi-transparent photovoltaic elements for building integration under real operation conditions. *Energy Build.* **2014**, *68*, 280–291. [\[CrossRef\]](#)
- Chae, Y.T.; Kim, J.; Park, H.; Shin, B. Building energy performance evaluation of building integrated photovoltaic (BIPV) window with semi-transparent solar cells. *Appl. Energy* **2014**, *129*, 217–227. [\[CrossRef\]](#)
- Peng, J.Q.; Curcija, D.C.; Lu, L.; Selkowitz, S.E.; Yang, H.X.; Zhang, W.L. Numerical investigation of the energy saving potential of a semi-transparent photovoltaic double-skin facade in a cool-summer Mediterranean climate. *Appl. Energy* **2016**, *165*, 345–356. [\[CrossRef\]](#)
- Elarga, H.; Zarrella, A.; De Carli, M. Dynamic energy evaluation and glazing layers optimization of facade building with innovative integration of PV modules. *Energy Build.* **2016**, *111*, 468–478. [\[CrossRef\]](#)
- Wang, C.Y.; Ji, J.; Uddin, M.M.; Yu, B.D.; Song, Z.Y. The study of a double-skin ventilated window integrated with CdTe cells in a rural building. *Energy* **2021**, *215*, 17. [\[CrossRef\]](#)
- Chow, T.T.; Fong, K.F.; He, W.; Lin, Z.; Chan, A.L.S. Performance evaluation of a PV ventilated window applying to office building of Hong Kong. *Energy Build.* **2007**, *39*, 643–650. [\[CrossRef\]](#)
- Wang, C.Y.; Li, N.S.; Yu, B.D.; Uddin, M.M.; Ji, J. A novel solar spectrum-splitting utilization photocatalytic CdTe double-skin facade: Concept, design and performance investigation. *Build. Environ.* **2021**, *195*, 16. [\[CrossRef\]](#)

29. Duffie, J.A.; Beckman, W.A. *Solar Engineering of Thermal Processes; Meteorological Data*; John Wiley & Sons, Inc.: Hoboken, NJ, USA, 2013; pp. 863–869. [[CrossRef](#)]
30. Li, G.Q.; Zhao, X.D.; Ji, J. Conceptual development of a novel photovoltaic-thermoelectric system and preliminary economic analysis. *Energy Conv. Manag.* **2016**, *126*, 935–943. [[CrossRef](#)]
31. Ong, K.S.; Chow, C.C. Performance of a solar chimney. *Sol. Energy* **2003**, *74*, 1–17. [[CrossRef](#)]
32. Khalvati, F.; Omidvar, A. Summer study on thermal performance of an exhausting airflow window in evaporatively-cooled buildings. *Appl. Therm. Eng.* **2019**, *153*, 147–158. [[CrossRef](#)]
33. Jle, J.; Hua, Y.; Wei, H.; Gang, P.; Lu, J.P.; Bin, J. Modeling of a novel Trombe wall with PV cells. *Build. Environ.* **2007**, *42*, 1544–1552. [[CrossRef](#)]
34. Skoplaki, E.; Palyvos, J.A. On the temperature dependence of photovoltaic module electrical performance: A review of efficiency/power correlations. *Sol. Energy* **2009**, *83*, 614–624. [[CrossRef](#)]
35. Jie, J.; Bin, J.; Huai, Y.; Tin-Tai, C.; Wei, H.; Gang, P. An experimental and mathematical study of efforts of a novel photovoltaic-Trombe wall on a test room. *Int. J. Energy Res.* **2008**, *32*, 531–542. [[CrossRef](#)]
36. Khalifa, A.; Marshall, R.H. Validation of heat transfer coefficients on interior building surfaces using a real-sized indoor test cell. *Int. J. Heat Mass Transf.* **1990**, *33*, 2219–2236. [[CrossRef](#)]
37. Xu, L.J.; Luo, K.; Ji, J.; Yu, B.D.; Li, Z.M.; Huang, S.J. Study of a hybrid BIPV/T solar wall system. *Energy* **2020**, *193*, 401–415. [[CrossRef](#)]

**Disclaimer/Publisher’s Note:** The statements, opinions and data contained in all publications are solely those of the individual author(s) and contributor(s) and not of MDPI and/or the editor(s). MDPI and/or the editor(s) disclaim responsibility for any injury to people or property resulting from any ideas, methods, instructions or products referred to in the content.